The Journal of Chemical Physics

Microscopic theory of singlet exciton fission. III. Crystalline pentacene

Cite as: J. Chem. Phys. **141**, 074705 (2014); https://doi.org/10.1063/1.4892793
Submitted: 27 May 2014 . Accepted: 30 July 2014 . Published Online: 18 August 2014

Timothy C. Berkelbach, Mark S. Hybertsen, and David R. Reichman

View Online Export Citation CrossMark

ARTICLES YOU MAY BE INTERESTED IN

Microscopic theory of singlet exciton fission. II. Application to pentacene dimers and the role of superexchange
The Journal of Chemical Physics **138**, 114103 (2013); https://doi.org/10.1063/1.4794427

Microscopic theory of singlet exciton fission. I. General formulation
The Journal of Chemical Physics **138**, 114102 (2013); https://doi.org/10.1063/1.4794425

Vibronic exciton theory of singlet fission. I. Linear absorption and the anatomy of the correlated triplet pair state
The Journal of Chemical Physics **146**, 174703 (2017); https://doi.org/10.1063/1.4982362

© 2014 AIP Publishing LLC.

THE JOURNAL OF CHEMICAL PHYSICS **141**, 074705 (2014)

Microscopic theory of singlet exciton fission. III. Crystalline pentacene

Timothy C. Berkelbach,[1,a)] Mark S. Hybertsen,[2,b)] and David R. Reichman[1,c)]
[1]*Department of Chemistry, Columbia University, 3000 Broadway, New York, New York 10027, USA*
[2]*Center for Functional Nanomaterials, Brookhaven National Laboratory, Upton, New York 11973-5000, USA*

(Received 27 May 2014; accepted 30 July 2014; published online 18 August 2014)

We extend our previous work on singlet exciton fission in isolated dimers to the case of crystalline materials, focusing on pentacene as a canonical and concrete example. We discuss the proper interpretation of the character of low-lying excited states of relevance to singlet fission. In particular, we consider a variety of metrics for measuring charge-transfer character, conclusively demonstrating significant charge-transfer character in the low-lying excited states. The impact of this electronic structure on the subsequent singlet fission dynamics is assessed by performing real-time master-equation calculations involving hundreds of quantum states. We make direct comparisons with experimental absorption spectra and singlet fission rates, finding good quantitative agreement in both cases, and we discuss the mechanistic distinctions that exist between small isolated aggregates and bulk systems.
© *2014 AIP Publishing LLC*. [http://dx.doi.org/10.1063/1.4892793]

I. INTRODUCTION

Singlet exciton fission is a spin-conserving energy transfer event whereby a photogenerated singlet exciton splits into two lower-energy triplet excitons.[1,2] When combined with a secondary absorbing material, this type of multiple exciton generation[3] can boost the maximal power conversion efficiency of a solar cell to 45%,[4] well above the Shockley-Queisser limit of 31%.[5] Despite a significant number of experimental[6–19] and theoretical[20–32] studies on a wide range of materials, the microscopic mechanism by which singlet fission takes place is still a matter of debate. The status of the field has been expertly summarized by Smith and Michl in Ref. 1 and more recently in Ref. 2.

Theoretical and computational contributions to a mechanistic understanding of singlet fission have almost entirely focused on pairs (or dimers) of chromophore molecules.[20,21,23,27,30–32] Although this two-molecule picture is indeed a minimal model for singlet fission, it must be questioned whether such a model is quantitatively—or even qualitatively—relevant for experimental investigations in crystalline materials. It must be kept in mind that essentially all reported experimental findings of rapid and efficient singlet fission occur in the crystal phase[10,11,13–19] whereas singlet fission in covalent dimers in solution has been reported with vanishingly small yield.[33,34] Between single molecules and bulk crystals, there exist large variations in basic experimental signatures of electronic energy levels, including ionization energies and absorption spectroscopies, which already hints at the potential differences between these two classes of materials.

This undeniable gap between theory and experiment can be largely attributed to the theoretical and computational challenges associated with large system sizes; a unified treatment of the static and dynamic properties of large systems of interacting electrons and phonons is an ongoing challenge in condensed phase chemical dynamics. For example, even the static *ab initio* energy ordering of the low-energy states of isolated acene dimers is still under debate.[21,24,30–32] This paper bridges this critical gap by extending our previous work on singlet fission in pentacene dimers[26,27] to the problem of singlet fission in *crystalline* pentacene, *treated at the same level of theory*. Our ability to treat such large system sizes originates from a more pragmatic computational approach that employs a careful combination of quantum chemical and semi-empirical methods guided by experiment. In this way, we are able to consistently compare our mechanistic predictions between dimers and crystals, and more importantly between theory and experiment. Furthermore, our theoretical framework continues to be the only one to microscopically treat the exciton dynamics in the presence of coupling to thermal vibrations. This latter feature is mandatory for any meaningful prediction of *rates*, which are the most robust experimental observables for singlet fission.

The layout of this paper is as follows. We begin in Sec. II with a summary that places the present work in the context of our previous work. This is followed in Sec. III by a review of the methodology relevant for a treatment of larger clusters and crystals. In Sec. IV, we present our results, focusing on the linear absorption, charge-transfer characterization, and singlet fission dynamics of crystalline pentacene. We conclude in Sec. V. An Appendix is devoted to a discussion of the validity of the diabatic approach to singlet fission used in this work.

II. SUMMARY OF MAJOR RESULTS

In the first paper[26] of this series (hereafter referred to as Paper I), we formulated a generic, microscopic theory of singlet fission, which unified static electronic structure and subsequent quantum dynamics in the presence of a

a)Electronic mail: tcb2112@columbia.edu
b)Electronic mail: mhyberts@bnl.gov
c)Electronic mail: drr2103@columbia.edu

 © 2014 AIP Publishing LLC

vibrational bath. In the second paper[27] (hereafter Paper II), we applied this formalism to the study of singlet fission dynamics in *pairs* of pentacene molecules. One aspect of Paper II[27] concerned the role, or lack thereof, of so-called charge-transfer (CT) states in the early stages of singlet fission as a means of generating a correlated triplet pair state (TT) from the initially photoexcited Frenkel excitation (FE). We found that for pentacene dimers the "direct," two-electron coupling is quite weak, capable of producing fission dynamics on a timescale no shorter than about 10 ps. We found that a higher-order superexchange-like singlet fission mechanism mediated by CT states, with an effective (second order) matrix element $V_{\text{eff}} = V_{FE,CT} V_{CT,TT}/\Delta E(CT)$, dominated the direct two-electron transfer process. This higher-order mechanism for singlet fission has since been adopted in a number of works.[2,29,31] However, in Paper II[27] it was demonstrated that a pure non-adiabatic rate theory based on the superexchange matrix element is not *quantitatively* accurate due to the fact that the matrix elements that control the mixing with CT states are of the same order as the energy difference between the FE and CT states themselves. In this large coupling limit, $V_{\text{eff}} > 10$ meV, our dynamics calculations showed the onset of a plateau in the singlet fission rate (see Fig. 7(b) of Paper II[27]). Remarkably this behavior, including even the value of the plateau onset, has been very recently observed in a large-scale joint experimental and theoretical study by Yost *et al.*[35] These authors rationalized their findings in a manner consistent with the theory presented in Paper II.[27]

In this paper we apply the methodology developed in Papers I[26] and II[27] to treat fission in bulk crystals, focusing on the prototypical case of pentacene. Hundreds of electronic states coupled to lattice (phonon) degrees of freedom are treated within a fully microscopic framework for the quantum dynamics following the initial photo-excitation of the bright, low-lying S_1 singlet state. On a superficial level, we find that the time-dependent populations of the S_1 and TT states in the pentacene crystal appear to proceed in a manner similar to that of an isolated pentacene dimer whose geometry is taken from the crystal (*vide infra*, compare Fig. 5 of this work and Fig. 5 of Paper II[27]). In particular, in both cases we find that the temporal growth of the TT state is ultrafast (occurring on the order of 250 fs) with nearly exponential kinetics. This fact would seem to support the notion that in studying fission kinetics, a dimer, perhaps embedded in a continuum dielectric environment, is a good proxy for the bulk. However, a closer analysis reveals that there are qualitative distinctions between dimers and crystals.

For a pentacene dimer, as described above, the coupling between the FE and TT states is enhanced by mixing with high-lying, virtual CT states. In the bulk case investigated here, we will clearly demonstrate that the FE and CT states are strongly mixed into the *adiabatic* S_1 state, a mixing facilitated by the lowering of CT energy levels engendered by the polarizability of the surrounding molecules. In this sense, the low-lying photoexcited singlet already has a large CT component. *Hence, fission in pentacene essentially occurs via a direct one-electron, as opposed to a two-electron, transfer process.* It should be noted however, that the degree of CT mixing is material dependent. Specifically, materials with small inter-chromophore spacing, large electronic coupling, and highly polarizable or high dielectric environments should be ideal candidates for such CT mixing. However, the subsequent fission amplitude is maximized for nearest-neighbor CT pairs, and so materials with small exciton binding energies leading to rapid dissociation and carrier diffusion will be less efficient fission materials. In systems with an intermolecular spacing larger than that of pentacene, it is expected that the two-electron coupling will eventually dominate over the terms responsible for CT mixing. In such systems fission may occur via a direct two-electron transfer mediated by the Coulomb operator. In Paper II,[27] we investigated such a scenario and predicted that in this case fission would proceed on time scales of tens of picoseconds or slower. This prediction also appears consistent with the experimental findings of Yost *et al.*[35]

With respect to the treatment of electronic structure, our theory—developed and applied in Papers I,[26] II,[27] and the present work—employs a real-space, tight-binding (diabatic) formulation. Here, adjustment of parameters is carried out to optimize agreement with aspects of the absorption spectrum, similar to the approach taken in earlier studies that targeted the Davydov shift.[28,36] General considerations pertaining to the validity of the diabatic approach to fission are discussed in the Appendix. The values of electronic coupling parameters that we find for pentacene are in semi-quantitative agreement with those found independently by block-localized DFT,[37] constrained DFT,[35] and both restricted[31] and complete[32] active space methods. In comparison with calculations for bulk pentacene at the GW and GW+Bethe-Salpeter equation levels of electronic structure theory, we find good agreement both with respect to the band structure (Fig. 1) and the qualitative real-space characteristics of the electron-hole distributions (Fig. 4).

We further provide a detailed analysis of the real-space electronic character of the S_1 state in Sec. IV B. Although the deficiency of assessing CT character via examination of static dipole moments has been discussed in several recent studies,[30,38,39] we make this point explicit by calculating dipole moments associated with low-lying singlet states for clusters derived from the crystal structure of pentacene. For clusters that break the natural inversion symmetry of the crystal (such as those employed in Ref. 22), a non-zero static dipole moment may be detected in low-lying singlet states, while clusters that obey the symmetry of the periodic crystal exhibit a vanishing dipole moment for all excited singlet states. This analysis makes clear that such dipole moments are not directly associated with CT character, but instead arise from surface-localized charge density in systems with broken symmetry. We will also explicitly show that for the assignment of CT character, as well as for quantification of the exciton size, the examination of the exciton correlation function provides more useful information than a natural transition orbital analysis in periodic crystals with inversion symmetry.

III. METHODOLOGY

Because our adopted theoretical methodology has been described and utilized in Papers I[26] and II,[27] we will only

briefly describe the formalism, with a focus on the differences between the present crystal-phase calculation and our previous study of acene dimers. We employ a system-bath excitonic Hamiltonian describing the coupling of the electron and phonon degrees of freedom,[40,41] $\hat{H}_{tot} = \hat{H}_{el} + \hat{H}_{el-ph} + \hat{H}_{ph}$, with

$$\hat{H}_{el} = \sum_i |i\rangle E_i \langle i| + \sum_{i\neq j} |i\rangle V_{ij} \langle j|, \tag{1}$$

$$\hat{H}_{el-ph} = \sum_i |i\rangle\langle i| \sum_k c_{k,i}\hat{q}_k + \sum_{i\neq j} |i\rangle\langle j| \sum_k c_{k,ij}\hat{q}_k, \tag{2}$$

and

$$\hat{H}_{ph} = \sum_k \left[\frac{\hat{p}_k^2}{2} + \frac{1}{2}\omega_k^2 \hat{q}_k^2\right]. \tag{3}$$

We emphasize that the Hamiltonian above is constructed in a basis of many-body electronic states. The parameters of this Hamiltonian are determined via a variety of *ab initio* and semi-empirical methods, as discussed in Sec. III B.

A. Reduced density matrix quantum dynamics

The reduced dynamics generated by the above Hamiltonian are calculated with a Redfield-type, weak-coupling quantum master equation.[26,40,42] Specifically, in the basis of electronic eigenstates $\hat{H}_{el}|\alpha\rangle = \hbar\omega_\alpha|\alpha\rangle$, the reduced density matrix (i.e., averaged over the phonon degrees of freedom) obeys the equation of motion

$$\frac{d\rho_{\alpha\beta}(t)}{dt} = -i(\omega_\alpha - \omega_\beta)\rho_{\alpha\beta}(t) + \sum_{\gamma,\delta} R_{\alpha\beta\gamma\delta}\rho_{\gamma\delta}(t). \tag{4}$$

Explicit expressions for the Redfield tensor, $R_{\alpha\beta\gamma\delta}$, which introduces population relaxation and coherence dephasing, can be found in Appendix C of Paper I.[26] Such expressions depend only on the spectral density of the phonons, which we take to be identical for all electronic states, and to be of the Ohmic form with a Debye cutoff, i.e.,

$$J(\omega) = \frac{\pi}{2}\sum_k \frac{c_k^2}{\omega_k}\delta(\omega - \omega_k) = 2\lambda\Omega\omega\frac{1}{\omega^2 + \Omega^2}. \tag{5}$$

We take $\lambda = 50$ meV and $\hbar\Omega = 180$ meV. Consistent with our findings in Paper II,[27] we neglect the off-diagonal Peierls coupling. As an aside, we would like to point out that the "true" spectral density as defined in the first equality of Eq. (5) has a maximum phonon frequency above which $J(\omega) = 0$ (roughly around 3000 cm^{-1} for C–H stretching modes in acenes). However, the addition of a high-frequency component to the spectral density, when treated to lowest order (as in Redfield theory), can serve as a proxy for multi-phonon relaxation processes arising from lower-energy phonons.[43,44] A more careful treatment would follow from writing the electron-phonon interaction more generically as $\hat{H}_{el-ph} = \sum_i |i\rangle\langle i|\Phi_i(\{q_k\})$, which need not be linear in the coordinates. The (generally temperature-dependent) spectral density is then understood to be related to the Fourier transform of the phonon autocorrelation function $\langle\Phi_i(\{q_k(t)\})\Phi_i(\{q_k(0)\})\rangle_{ph}$, which will include a high-frequency tail arising from lowest-order scattering events in the nonlinear components of the exciton-phonon coupling term Φ_i. Alternatively, the high-frequency tail could be interpreted as an approximate treatment of higher-order scattering events in the linear exciton-phonon coupling, which is neglected in Redfield theory but could be included with modified Redfield theory[44,45] or polaronic master equations.[46,47] In Ref. 48, we combined lowest-order Redfield theory with a model for the nonlinear exciton-phonon coupling to more accurately treat multiphonon relaxation in crystalline hexacene, which is a highly exothermic singlet fission material.

With large quantum dynamics calculations in mind, let us briefly comment on aspects of computational tractability. First and foremost, a reduced density matrix calculation is likely the *only* microscopic quantum dynamics formalism with the potential to scale to large clusters approaching crystal behavior, primarily because such an approach has already averaged over the continuous vibrational degrees of freedom. Without invoking the secular approximation (which decouples population and coherence evolution in the electronic eigenstate basis), the solution of the Redfield equation requires the application of the $N^2 \times N^2$ Redfield tensor onto the $N \times N$ density matrix (where N is the number of electronic states). Such an effective matrix-vector multiplication scales as $O(N^4)$. Pollard and Friesner[49] showed that by exploiting the structure of most system-bath interactions, the application of the Redfield tensor can be reduced to B matrix-matrix multiplications, scaling as $O(BN^3)$, where B is the number of collective bath variables to which the system is coupled (and can be as few as $B = 1$). In the case where each electronic state is coupled to its own set of bath variables, then $B = N$, and there is no *operational* savings in the Pollard and Friesner scheme;[49] even worse, in the presence of Peierls-like off-diagonal coupling to $B = N^2$ independent sets of bath variables, it scales as $O(N^5)$, which is *worse* than the naive approach. However, this scheme never requires the storage of the Redfield tensor and so there can indeed be savings in memory storage requirements, depending on implementation. In our calculations, we have exploited the techniques of Pollard and Friesner,[49] which were sufficient to treat the desired system sizes. Furthermore, the results presented have invoked the secular approximation, although the non-secular Redfield dynamics exhibit the same qualitative behavior.[26]

B. Geometry and electronic structure

Following Paper I,[26] we parameterize our electronic Hamiltonian in a tight-binding basis of localized, diabatic states with excitations spanning one or two molecules per basis state. The basis states are characterized as being in one of three spin singlet classes: (1) intramolecular FE; (2) intermolecular CT; and (3) correlated TT. Note that in Papers I[26] and II,[27] we followed the convention of the field and referred to localized FE states as S_1 states. We avoid this potentially confusing nomenclature here because the lowest-lying (adiabatic) singlet excitation in crystals is no longer dominated by FE states, *vide infra*.

For a cluster of M molecules, there are in principle M FE states, $M(M-1)$ CT states, and $M(M-1)/2$ TT states, such that the number of states grows quadratically with the number of molecules, i.e., $N \sim M^2$. However, in molecular crystals like pentacene, the molecules largely retain their isolated properties and intermolecular interactions are reasonably weak, suggesting a semi-empirical truncation of the excitations to nearest-neighbors only (allowing for weakly Wannier-like excitons). With this approximation, the number of electronic states grows linearly with M. Our Hamiltonian is thus given by $\hat{H}_{el} = \hat{H}_{FE} + \hat{H}_{CT} + \hat{H}_{TT} + \hat{H}_{FE,CT} + \hat{H}_{CT,TT}$, where

$$\hat{H}_{FE} = \sum_m |FE_m\rangle E_{FE} \langle FE_m|, \tag{6}$$

$$\hat{H}_{CT} = \sum_{\langle mn\rangle} |C_m A_n\rangle E_{CT}(m,n) \langle C_m A_n|, \tag{7}$$

$$\hat{H}_{TT} = \sum_{\langle mn\rangle} |T_m T_n\rangle E_{TT} \langle T_m T_n|, \tag{8}$$

$$\hat{H}_{FE,CT} = \sum_{\langle mn\rangle} [|FE_m\rangle t_{LL}(m,n) \langle C_m A_n| - |FE_m\rangle t_{HH}(m,n) \langle C_n A_m| + H.c.], \tag{9}$$

$$\hat{H}_{CT,TT} = \sqrt{3/2} \sum_{\langle mn\rangle} [|T_m T_n\rangle t_{HL}(m,n) \langle C_m A_n| + |T_m T_n\rangle t_{LH}(m,n) \langle C_n A_m| + H.c.], \tag{10}$$

where $\langle mn\rangle$ denotes that m and n are nearest-neighbors. We have neglected the so-called "direct" coupling, two-electron matrix element $\langle FE_m|\hat{H}_{el}|T_m T_n\rangle$ due to its relative smallness, as quantified statically and dynamically in Paper II.[27] It is straightforward to include this contribution if necessary.

The molecules in a pentacene crystal adopt a familiar herringbone packing arrangement. As discussed in Paper II,[27] there are approximately three symmetry-unique nearest-neighbor pairs of molecules with different electronic interactions. Following the Appendixes of Paper I,[26] we employ notation such that ε_g is the single-molecule HOMO-LUMO gap *in the crystal environment* and $t_{AB}(m,n)$ are one-electron coupling matrix elements (H and L denote the HOMO and LUMO). These properties follow from an appropriate one-electron theory, for which we have used Hartree-Fock theory, supplemented with renormalizations appropriate for the crystal. Specifically, ε_g must be significantly reduced from the gas phase value and the one-electron couplings t_{AB} are rescaled to incorporate screening effects. Importantly, the relative magnitudes and phases of the symmetry-distinct electronic couplings are meaningful and are retained in the calculation. In the absence of electron-hole interaction effects, these parameters yield the single-particle band structure shown in Fig. 1, which is in good agreement with previously published *ab initio* GW calculations.[50] Although the LUMO band in particular shows slightly less dispersion than that obtained by GW,

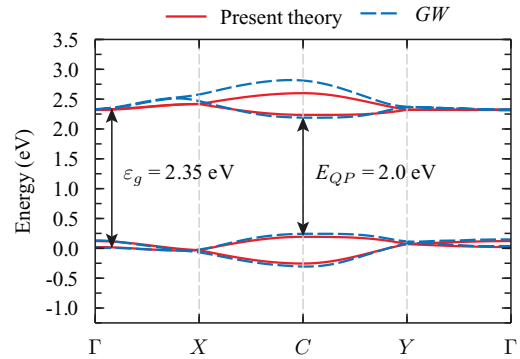

FIG. 1. Band structure of crystalline pentacene calculated within the present theory compared to the many-body GW results of Ref. 50. Also shown are the bare single-molecule gap ε_g in the absence of dispersion, and the minimum quasiparticle gap E_{QP} when dispersion is included.

our approach yields an absorption spectrum in better agreement than that from GW plus the Bethe-Salpeter equation (BSE). Furthermore, the quasiparticle gap of $E_{QP} = 2.0$ eV, located at the C-point in the Brillouin zone, is in good agreement with the experimental value of 2.2 eV,[51,52] especially when accounting for surface effects. The reduction as compared to the gas-phase single molecule gap of about 5 eV[53] can be ascribed to electronic polarization of the surrounding crystal medium.

Electron-hole interaction effects are incorporated with a configuration interaction approach, from which we write the diagonal energies as

$$E_{FE} = \varepsilon_g + 2K - J, \tag{11}$$

$$E_{CT}(i,j) = \varepsilon_g - J'(i,j), \tag{12}$$

$$E_{TT} \approx 2E(T) = 2(\varepsilon_g - J). \tag{13}$$

In the above,

$$J = \int d^3\mathbf{r}_1 \int d^3\mathbf{r}_2 H_A^2(\mathbf{r}_1) r_{12}^{-1} L_A^2(\mathbf{r}_2) \tag{14}$$

is a direct, intramolecular Coulomb integral;

$$K = \int d^3\mathbf{r}_1 \int d^3\mathbf{r}_2 H_A(\mathbf{r}_1) L_A(\mathbf{r}_2) r_{12}^{-1} L_A(\mathbf{r}_1) H_A(\mathbf{r}_2) \tag{15}$$

is an intramolecular exchange integral; and

$$J_1' = \int d^3\mathbf{r}_1 \int d^3\mathbf{r}_2 H_A^2(\mathbf{r}_1) r_{12}^{-1} L_B^2(\mathbf{r}_2), \tag{16}$$

$$J_2' = \int d^3\mathbf{r}_1 \int d^3\mathbf{r}_2 H_B^2(\mathbf{r}_1) r_{12}^{-1} L_A^2(\mathbf{r}_2) \tag{17}$$

are direct, intermolecular Coulomb integrals. For simplicity, we assume $J_1' = J_2' \equiv J'$ (although we point out that very recently Zeng *et al.*[32] have shown that this is not accurate for certain molecular geometries). We have neglected the intermolecular exchange integral due to the smallness of the differential overlap. We adopt the Bethe-Salpeter viewpoint to

TABLE I. Electronic structure values (all in eV, except t_{ij} in meV) for the pentacene crystal for monomers (top) and for the three nearest-neighbor dimer types (bottom). All values should be understood to be in the crystal environment, not the gas phase.

	ε_g	J	$E(T_1)$	$2K$	$E(FE)$	
Monomer	2.35	1.45	0.90	1.10	2.0	
[a b]	J'	$E(CT)$	t_{HH}	t_{LL}	t_{HL}	t_{LH}
[1 0]	0.10	2.25	26	−24	−26	26
[1/2 1/2]	0.30	2.05	−44	46	38	−43
[−1/2 1/2]	0.35	2.00	68	−44	38	−47

configuration-interaction excitations, such that K is an unscreened exchange integral, whereas J and J' are screened direct integrals.[54] With this convention, K approximately satisfies the experimental, single-molecule singlet-triplet exchange splitting, $2K \approx E(S_1) - E(T_1)$ which we take to be 1.10 eV.[55,56] The unscreened direct interaction for a gas-phase molecule would be $J \approx E_g - E(T_1) \approx 4$ eV, however, it is reduced in the crystal by approximately a factor of 3 due to screening, and we use $J = 1.45$ eV. The value of J', which sets the CT state energies, depends on the specific dimer-pair, and is accordingly larger for nearer neighbors (stronger electron-hole interaction). Our employed CT state energies are in good agreement with those obtained experimentally by Sebastien *et al.*[57] and theoretically by Yamagata *et al.*[36] The values for all parameters used throughout this work are collected in Table I.

The ultimate validation of these parameters lies in the theoretically predicted absorption spectrum which includes all the effects of state-mixing and spatial delocalization. We turn to this topic next. In all results presented henceforth, we have performed calculations on finite clusters of $N = 10$, 27, and 52 molecules (roughly 3×3, 5×5, and 7×7, respectively) until converged. Without the Hilbert space truncation described above (i.e., nearest-neighbor CT and TT pairs only), these clusters would have 145, 1080, and 4030 electronic states. With such truncation, these clusters have 67, 213, and 439 electronic states, which still provide significant computational demands in light of the scaling of density matrix dynamics described above.

IV. RESULTS

A. Linear absorption spectroscopy

A crucially important metric in assessing the accuracy of the employed electronic structure model is the calculated linear absorption signal. Furthermore, because of the anisotropy of the pentacene herringbone lattice, polarized absorption spectroscopy permits access to more detailed structural information. Specifically, we calculate the imaginary part of the dielectric function

$$\varepsilon_2(\omega) \propto \frac{1}{\omega^2} \sum_\alpha |\mathbf{e} \cdot \boldsymbol{\mu}_\alpha|^2 D(E_\alpha - \hbar\omega), \tag{18}$$

where $D(E)$ is a lineshape function (taken to be Gaussian with a broadening of 0.04 eV), $\mathbf{e}$ is the optical polarization vector,

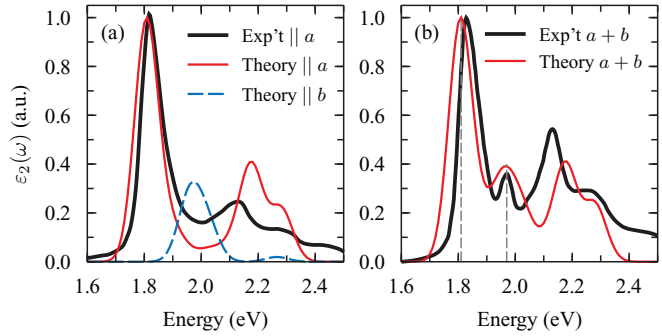

FIG. 2. Comparison between theoretically predicted and experimental absorption spectra of crystalline pentacene. Panel (a) shows the theoretical spectrum for both a and b polarization, compared to the experimental a-polarized spectrum from Ref. 59. Panel (b) compares the theoretical averaged spectrum with that of a polycrystalline sample given in Ref. 17, where we have converted absorption data via $\varepsilon_2(\omega) \propto \alpha(\omega)/\omega$. All spectra are normalized to the peak value of the lowest-lying transition. The Davydov shift is given by the energy separation of the first two peaks in panel (b), as emphasized by the vertical dashed lines.

and

$$\boldsymbol{\mu}_\alpha \approx \langle 0|\hat{\boldsymbol{\mu}}|\alpha\rangle = \sum_n C^\alpha_{FE_n} \boldsymbol{\mu}_{FE} \tag{19}$$

is the transition dipole moment to the adiabatic excited state α. Note that we assume that the localized Frenkel exciton states carry all the oscillator strength, and thus the optical brightness of a given adiabatic excited state is dependent on the degree of Frenkel exciton character. The absorption (or extinction) coefficient $\alpha(\omega)$ is related to the dielectric function via $\alpha(\omega) \propto \omega\varepsilon_2(\omega)$, where the index of refraction is assumed constant over the energy range of interest.

To assess our electronic structure model, we seek to compare to experimental measurements whenever possible. Unfortunately, experimental polarization-resolved absorption spectra for pentacene are in fact quite varied. This may in part be due to variations in methodology necessitated by crystal anisotropy, which include reflectivity,[58] generalized ellipsometry,[59] and electron energy-loss spectroscopy.[58,60,61] Spectra for the a-polarized absorption are more uniform, and in Fig. 2(a) we compare to the ellipsometry spectrum from Ref. 59. The total absorption spectrum, i.e., the average of the $a + b$ components, can be obtained from polycrystalline samples. In Fig. 2(b), we compare to low temperature (4 K) absorption spectra of such a polycrystalline film presented in Ref. 17. The agreement for all observed peaks can be seen to be quite good, giving credence to our employed electronic structure model. In Ref. 61, it was remarked that the structure in pentacene's a-polarized spectrum does not appear to originate from a vibronic progression, in contrast to that of tetracene and smaller acenes. This observation is consistent with our calculation, which neglects explicit phonon coupling in the absorption spectra. Such behavior can be understood in terms of the reduced exciton-phonon coupling in larger molecules, combined with an increased CT-mixing that accounts for the additional peaks (discussed further below).

Importantly, such polarization-resolved spectra offer access to the Davydov shift, i.e., the signed difference between the first peaks of the b- and a-polarized spectra. Our

calculations yield a Davydov shift of 0.16 eV, in good agreement with various experimental values (0.13 eV,[17,62,63] 0.14 eV,[64] and 0.15 eV[59]) and theoretical values (0.13 eV[28,36,50] and 0.20 eV[65]). Yamagata *et al.*[36] have identified an important trend in their theoretical study of acene spectroscopy: an increasing (positive) Davydov shift is correlated with an increasing degree of CT character *physically mixed* into the low-lying bright S_1 exciton. Indeed, in our calculations on sufficiently large clusters of pentacene molecules, we find that the lowest-lying, bright singlet state comprises roughly 50% FE and 50% CT character. These observations are consistent with the CT exciton characteristics inferred from solid-state GW+BSE calculations on periodic pentacene crystals,[38,50,65] but inconsistent with recent quantum chemical TD-DFT calculations on finite pentacene clusters embedded in a polarizable environment.[22] Given the important prospective role of CT states in facilitating rapid singlet fission, we now turn to an analysis of CT character, seeking to unify the theoretical results put forth to date.

B. Characterizing charge-transfer character

Because of the localized basis employed in our electronic structure model, we can definitively quantify the degree of CT character (∼50%) in our adiabatic excited states (and likewise in the work of Yamagata *et al.*[36] and Beljonne *et al.*[28]). However, in *ab initio* approaches that work directly in the adiabatic basis, such as TD-DFT or GW+BSE, no such decomposition is possible. Thus, to put our work in perspective, we will consider more generic quantities which are in principle available to all levels of theory. Specifically, we will consider three possible metrics for characterizing CT character: the static dipole moment of an excited state, natural transition orbitals (NTOs), and exciton correlation functions.

Let us first briefly consider the static dipole moment, as was used in Ref. 22 to argue against CT character in low-lying excited states of tetracene and pentacene. Specifically, the authors of that work found a small dipole moment for low-lying excited states but a larger dipole moment for high-lying excited states, and from this concluded that low-lying states were of Frenkel type and only high-lying states had significant CT character. Although such an analysis is useful in asymmetric small molecules (such as metal-to-ligand charge transfer[66]), for symmetric systems (like periodic crystals) there can be no *net* charge-transfer in any direction, as this would break symmetry. We believe the nonzero dipole moments of Ref. 22 are only due to the use of a finite cluster which breaks the inversion symmetry inherent in the crystal. This concern has been raised in a number of other recent works.[38,39] To demonstrate this assertion, we performed *ab initio* HF+CIS calculations with a modest 6-31G(d) basis set on two different molecular clusters of pentacene (calculations were carried out at the experimental geometry with the GAMESS(US) software package[67]). The first is the four-molecule cluster considered in Ref. 22 and the second is a seven-molecule cluster which restores inversion symmetry, as shown in Fig. 3. The dipole moments of the first five excited states for each cluster are given in Table II. Clearly, the four-molecule cluster exhibits large and increasing dipole moments which are completely absent in the inversion-symmetric seven-molecule cluster. We therefore conclude that a dipole-moment based analysis fails to report on CT character in solid-state materials, and turn now to the other two common metrics: NTO analysis and exciton correlation functions.

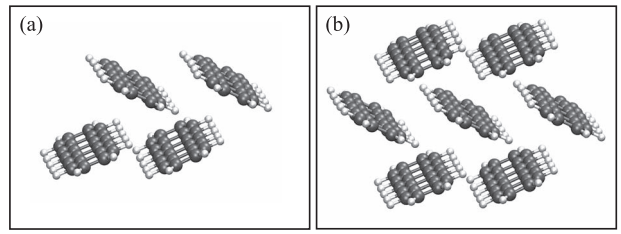

FIG. 3. Two finite molecular clusters considered for an evaluation of the static dipole moment as a measurement of CT character. The cluster shown in (a) was the one used in Ref. 22, however only the cluster in (b) preserves the inversion symmetry of the crystal. Calculated *ab initio* dipoles moments of the excited states are given in Table II.

The NTO analysis[68] is common in quantum chemistry and was employed in Ref. 22 as a second means of characterizing CT character for singlet fission materials. Exciton (electron-hole) correlation functions are more common in the solid-state GW+BSE community for such characterization.[54] Here we unify these two viewpoints in terms of the transition density matrix, relevant for any single-excitation theory (HF+CIS, TD-DFT, GW+BSE).

Consider the lowest lying bright excited state, S_1. Within a single-excitation theory, and employing a minimal, localized basis of HOMO (H) and LUMO (L) orbitals (M each), we can write

$$|S_1\rangle = \sum_{m,n} T_{mn} \hat{E}_{nm} |GS\rangle, \tag{20}$$

where the singlet excitation operator is given by $\hat{E}_{nm} = (c^\dagger_{L,n,\alpha} c_{H,m,\alpha} + c^\dagger_{L,n,\beta} c_{H,m,\beta})/\sqrt{2}$. The transition density matrix $T_{mn} = \langle GS|\hat{E}_{mn}|S_1\rangle$ is $M \times M$ and reflects the weight of excitation from the HOMO of molecule m to the LUMO of molecule n. In other words, the diagonal of the matrix corresponds to Frenkel excitations and the off-diagonal to CT excitations. Such an interpretation is not so straightforward in the basis of delocalized ground-state (HF-like) orbitals.

Calculating NTOs first requires rotating the transition density matrix from the localized basis to the HF-like basis: $\mathbf{T}' = \mathbf{C}_H \mathbf{T} \mathbf{C}_L^\dagger$, where $[\phi_L^{HF}]_i = \sum_j [\mathbf{C}_L]_{ij} [\phi_L^{loc}]_j$ and likewise for the HOMOs. The NTOs then result from a singular-value decomposition $\mathbf{U}\mathbf{T}'\mathbf{V}^\dagger = \Lambda$. The matrix $\mathbf{U}$

TABLE II. Total static dipole moments (in Debye) of the ground state and first five excited states for the 4- and 7-molecule clusters shown in Fig. 3.

	S_0	S_1	S_2	S_3	S_4	S_5
4-molecule cluster	0.0	0.5	3.6	16.5	23.0	15.7
7-molecule cluster	0.0	0.0	0.0	0.0	0.0	0.0

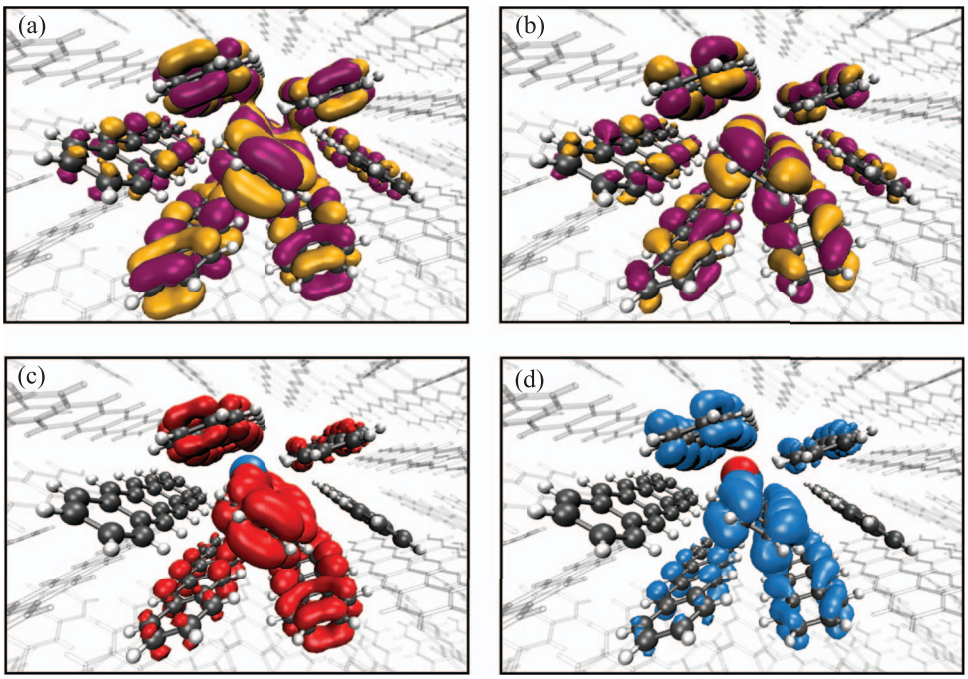

FIG. 4. Panels (a) and (b) depict, for the lowest-lying bright excited singlet state, the dominant natural transition orbitals of the electron and hole, respectively, projected onto a central cluster for clarity (these orbitals in reality extend over the entire system). The positive and negative phases of the orbitals are colored purple and orange, respectively. Despite the apparent spatial overlap, the excitation still has significant CT character. Panels (c) and (d) depict, for the same state, the electron and hole density for a fixed hole and electron position, respectively, where red is the electron density and blue is the hole density. The fixed hole and electron, depicted by the blue and red spheres, are located near the central molecule. Density on neighboring molecules unambiguously demonstrates significant CT character.

defines a transformation of the occupied orbitals into a set of NTOs representing the hole, and likewise **V** defines a transformation of the unoccupied orbitals into a set of NTOs representing the excited electron. The pair of electron and hole NTOs corresponding to the largest element of the diagonal matrix Λ gives, in some sense, the best electron-hole picture of the excited state, i.e.,

$$|S_1\rangle = \frac{\Lambda_{00}}{\sqrt{2}}\left(a^\dagger_{L,0,\alpha}a_{H,0,\alpha} + a^\dagger_{L,0,\beta}a_{H,0,\beta}\right)|GS\rangle + O(\Lambda_{11}), \tag{21}$$

where $a^\dagger_{L,n,\sigma} = \sum_v V_{nv}c^\dagger_{v,\sigma}$ and $a_{H,n,\sigma} = \sum_o U_{no}c_{o,\sigma}$.

Turning now to the use of exciton correlation functions, we consider the wavefunction of an electron-hole excitation in real space,

$$\chi_{S1}(\mathbf{r}_e, \mathbf{r}_h) = \sum_{m,n} T_{mn}L_n(\mathbf{r}_e)H_m(\mathbf{r}_h) = \sum_{v,c} T'_{vc}\phi_c(\mathbf{r}_e)\phi_v(\mathbf{r}_h), \tag{22}$$

where v and c denote valence and conduction bands; the latter equality is to emphasize that (unlike NTOs), the exciton wavefunction is independent of the choice of reference. This two-particle wavefunction is six-dimensional but can be visualized in three dimensions by fixing (for example) the hole near molecule A and plotting the electron density, $|\chi_{S1}(\mathbf{r}_e;\mathbf{r}_h = \mathbf{R}_A)|^2$, where

$$\chi_{S1}(\mathbf{r}_e;\mathbf{r}_h = \mathbf{R}_A) \approx H_A(\mathbf{R}_A)\sum_n T_{An}L_n(\mathbf{r}_e), \tag{23}$$

and we have utilized the locality of the MOs. In this way, one *correlates* the locations of the particle pair. Importantly, if the exciton is completely of Frenkel type, then the transition density matrix is completely diagonal (in the localized basis), $T_{An} = T_{AA}\delta_{An}$, and

$$\chi_{S1}(\mathbf{r}_e;\mathbf{r}_h = \mathbf{R}_A) \approx T_{AA}H_A(\mathbf{R}_A)L_A(\mathbf{r}_e) \propto L_A(\mathbf{r}_e). \tag{24}$$

Thus the electron density, *for a hole fixed near one molecule*, will be simply proportional to the (squared) LUMO orbital *on the same molecule*. In contrast, if the exciton is completely of the CT type, then the transition density matrix is entirely off-diagonal, $T_{An} = T_{An}(1 - \delta_{An})$, and

$$\chi_{S1}(\mathbf{r}_e;\mathbf{r}_h = \mathbf{R}_A) \approx H_A(\mathbf{R}_A)\sum_{n\neq A} T_{An}L_n(\mathbf{r}_e). \tag{25}$$

In this case, the electron density will be proportional to the sum of the squared LUMO orbitals on *neighboring* molecules. Again, although this interpretation is made most apparent in the localized basis, the exciton wavefunction and thus the analysis, is completely independent of basis.

In Fig. 4, *for the same excited state*, we compare the dominant electron and hole NTOs (panels (a) and (b)) with the electron and hole correlation functions, for fixed hole and electron, respectively (panels (c) and (d)). We find that the NTOs are extended over the entire system, and so for clarity we only plot the components on a central seven-molecule cluster. For the exciton correlation functions, these seven molecules are sufficient because in our model, CT excitations are restricted to nearest-neighbors only. As a reminder, the excited state under consideration has a 50%/50% mix of FE and CT components. Looking first at the NTOs, we see that they are both completely delocalized over the entire cluster, and show no electron-hole correlation. However, in contrast to the

claims of Ref. 22, this has no implication for CT character. Such a result is especially apparent here because we know the exciton wavefunction being analyzed has significant CT character, due to our use of a localized basis. We are forced to conclude again that NTO analysis, although useful for asymmetric molecules and excitations with a net transfer of charge,[68] is not useful for inversion symmetric or periodic systems, just as we found for the static dipole moment above.

On the contrary, if we look at the exciton correlation functions in Figs. 4(c) and 4(d), we clearly see evidence of both FE and CT character. As explicated above, the electron density on the same molecule as the (fixed) hole reports on FE components, whereas the electron density on neighboring molecules signals significant CT mixing (and vice versa for the hole density for fixed electron). In particular, we find significant CT excitations along the [−1/2 1/2] direction, which can be traced back to the low energy of these states and the strong coupling in this direction (see Table I). These latter points are also reflected in the anisotropic mobility tensor of acene crystals.[69]

This behavior is qualitatively similar, although quantitatively different, than that observed in analogous plots obtained via early GW+BSE[50] calculations, where essentially all electron density is on neighboring molecules, indicating a nearly pure CT exciton. However, our results appear to be similar to more recent calculations at the same level of theory.[65,70] To the extent that the transition dipole moment is purely intramolecular, i.e., $\langle H_m|\mathbf{r}|L_n\rangle = \delta_{mn}\boldsymbol{\mu}_{FE}$, the brightness of a singlet excited state is proportional to its FE character (as mentioned in Sec. III). Thus a pure CT exciton would be nearly dark spectroscopically, and so differences in the spatial exciton wavefunction may originate from different choices of the analyzed excited state, i.e., perhaps GW+BSE predicts low-lying, dark CT excitons, while the bright excitons necessarily have more FE character. For these reasons, we believe our analysis shown in Fig. 4 is generic for the lowest-lying *bright* exciton, independent of methodology.

As an aside, we would like to address some occasional confusion in the literature regarding the "size" of an exciton. In the absence of exciton-phonon coupling and crystal defects, there is no symmetry-breaking mechanism such that the crystal momentum is a good quantum number. Therefore, in terms of the *center-of-mass* degree of freedom, the exciton is delocalized over the entire system. This behavior is reflected in the NTO analysis presented in Figs. 4(a) and 4(b), as the electron and hole NTOs are completely delocalized (as observed in Ref. 22). More generally, the exciton's center-of-mass degree of freedom will exhibit localization dictated by any experimental or computational boundaries. In periodic systems, a more meaningful quantity is the exciton radius associated with the exciton's *relative* degree of freedom. Such an average electron-hole separation is the variable used in Wannier-like models of excitons, wherein the electron (or hole) is fixed at the origin giving rise to hydrogenic wavefunctions and energy relations. This symmetry-breaking imposed by fixing one of the two particles is exactly the same as that employed in the correlation function analysis presented in Figs. 4(c) and 4(d). Sharifzadeh *et al.*[38] have developed a variety of other useful metrics for assessing CT character, and similarly conclude that low-lying excitons in pentacene exhibit significant CT character, with average electron-hole separations greater than 6 Å.[38]

Let us conclude this section by emphasizing that, in light of the provisos explained above, the electronic structure calculations of Ref. 22 are in no way inconsistent with significant CT character in the low-lying excited states of tetracene and pentacene. We therefore anticipate that when analyzed carefully and consistently, most electronic structure calculations in the literature (semiempirical, TDDFT, or GW+BSE) would be in qualitative agreement concerning the role of CT mixing into low-lying, bright singlet states of larger oligoacenes. With this apparent discrepancy resolved, and having found strong evidence for significant CT character in these excited states, let us turn to the dynamical implications for the subsequent singlet fission.

C. Singlet fission dynamics

As an idealized initial condition, we first consider an excitation to the single lowest-lying, bright adiabatic eigenstate. Although an electronic eigenstate, this initial condition is nonstationary with respect to the nuclei (alternatively, it is a superposition in the localized, diabatic basis) and thus the relaxation dynamics will proceed towards thermalization. The results of our Redfield master equation dynamics are shown in Fig. 5(a); specifically we plot the summed population of all single excitations (FE+CT) and the summed population of all TT excitations. Furthermore, we decompose the single excitons into their FE and CT components; as described above, the initial condition is roughly 50%/50% in its FE/CT composition. As the dynamics proceed, the adiabatic S_1 state is depleted and the TT state is populated with a time constant of 270 fs, in qualitatively good agreement with the experimental value of 80–110 fs,[10,11,17] especially given the complexity of the process. We have verified that minor changes to the electronic structure or phonon spectral density could easily account for this difference. For example, a rescaling of the electronic couplings to larger values is capable of improving the rate, however this increases the single-particle bandwidth (Fig. 1) as well as the overall energy range of the absorption spectrum (Fig. 2). More trivially, a factor of two increase in the reorganization energy λ (strength of the exciton-phonon coupling) gives essentially quantitative agreement, because the Redfield theory rate roughly scales linearly with λ. This stronger coupling may actually be more physical, as we found in our calculation of the single-molecule absorption of pentacene in Paper I.[26] However, in this regime the weak-coupling Redfield dynamics would become unreliable (and the correct dynamics will likely show a turnover in the rate), which is why we have tried to remain in the weak-coupling limit (as discussed in Paper II[27]). Nonetheless, such a larger choice of λ would produce a parameter set for which our approach yields (uncontrolled) agreement with all studied experimental data. It will be interesting to see whether future improvements in the calculation of these input parameters can yield rates with quantitative accuracy.

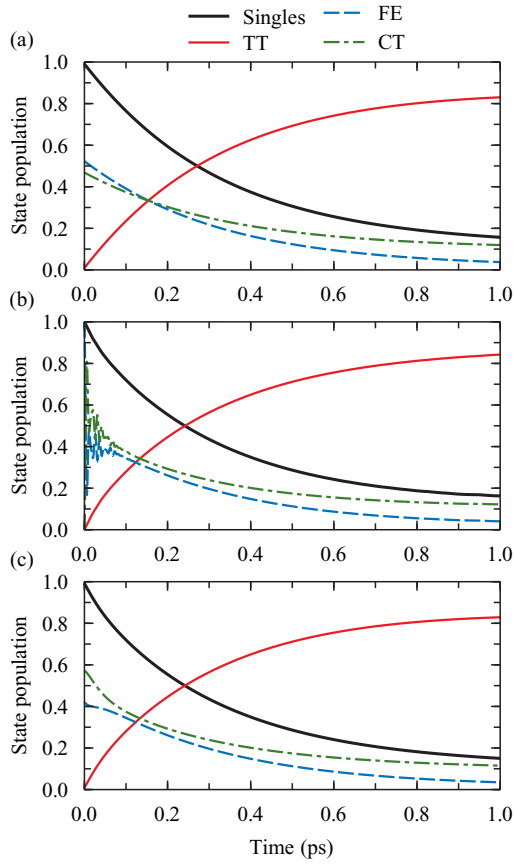

FIG. 5. Singlet fission population dynamics for all single excitations (thick black line), TT excitations (thinner red line), FE excitations (dashed blue line), and CT excitations (dotted-dashed green line). Note that the singles population is simply the sum of the FE and CT populations. Panel (a) is for an initial condition which populates only a single, low-lying bright adiabatic state (near 1.8 eV), panel (b) is for an impulsive (wide band) spectroscopic preparation which generates a coherent superposition of all molecular Frenkel excitations, and panel (c) is for an incoherent initial condition where all adiabatic states are populated proportional to their oscillator strength.

With regards to the underlying mechanism, we emphasize that because the initial condition already contains a significant degree of CT character, the low-energy TT states can be rapidly accessed via localized one-electron transfer events throughout the crystal, as was also suggested in Ref. 28. However, as mentioned in Sec. II, too much long-ranged CT character (i.e., Wannier excitons with a large exciton radius) is detrimental for singlet fission because such states are weakly coupled to the multiexciton triplet-pair manifold. We emphasize again that in spite of the similarity in timescales, the mechanisms for CT-mediated singlet fission in dimers (presented in Paper II[27]) and crystals (presented here) are qualitatively different. Nonetheless, we again find dynamics which appear "direct" in the one-step, kinetic sense. One must simply be careful in recognizing that the low-energy states accessed by photoexcitation are *not* of the pure FE type (although see next paragraph) and so concerns regarding two-electron transfer processes are unnecessary (at least for crystalline materials with sufficient CT character in their low-lying excited states).

We now consider a more realistic spectroscopic preparation[41] in the presence of a radiation field with Hamiltonian

$$\begin{aligned} H_{rad} &= -\sum_n \boldsymbol{\mu}_{FE} \cdot \mathbf{E}(t)[|FE_n\rangle\langle 0| + |0\rangle\langle FE_n|] \\ &= -\sum_\alpha \boldsymbol{\mu}_\alpha \cdot \mathbf{E}(t)[|\alpha\rangle\langle 0| + |0\rangle\langle \alpha|], \end{aligned} \tag{26}$$

where we again assume, as in Eq. (18), that the localized Frenkel-exciton basis states carry all of the oscillator strength. Additionally, α is an eigenstate of the electronic Hamiltonian (i.e., an adiabatic excited state at the ground-state geometry), $\boldsymbol{\mu}_\alpha = \langle 0|\hat{\boldsymbol{\mu}}|\alpha\rangle$ is the transition dipole moment (vector) from the ground state to the excited state α, and $\mathbf{E}(t)$ is the polarized time-dependent electric field. Henceforth we consider a-polarized fields, i.e., $\mathbf{E}(t) = E(t)\hat{\mathbf{x}}$. In the impulsive limit, $E(t) = A\delta(t)$, we imagine generating a *coherent* superposition of all localized FE states,

$$\rho_{FE_m,FE_n}(0) = \frac{1}{\hbar^2}|\mu_{FE,x}A|^2. \tag{27}$$

Therefore, strictly speaking, in the approximate limit where diabatic CT states are completely dark and FE states are bright, an impulsive excitation only populates the FE states. However, due to the non-zero coupling to CT states, this coherent initial condition very quickly evolves (on a femtosecond timescale) into a mixture of FE+CT states, which ultimately populate the TT state. This behavior is shown in Fig. 5(b). The laser pulse width required to resolve the observed coherent beating would be incredibly short. A simpler initial condition which accounts for a finite pulse width can be obtained by rotating the above reduced density matrix into the adiabatic (exciton) basis, and then neglecting the coherences under the assumptions of rapid decoherence,

$$\rho_{\alpha\alpha}(0) \approx \frac{1}{\hbar^2}|\mu_{\alpha,x}A|^2, \qquad \rho_{\alpha\neq\beta}(0) = 0. \tag{28}$$

The results of such preparation are shown in Fig. 5(c), which can be seen to accurately capture the behavior of Fig. 5(b), while averaging over the high-frequency coherence. In this scenario, the exciting pump pulse essentially has an infinite spectral bandwidth, populating all excited states in proportion to their oscillator strength, and thus giving a large non-zero CT component at time zero. For simplicity, in the above two results, we have chosen A to give the initial reduced density matrix unity trace.

Although the short time, transient dynamics of the individual FE and CT populations are slightly different when comparing Figs. 5(a) and 5(c) (in fact, the latter initial condition has *more* CT character), it is clear that the overall dynamics are qualitatively unchanged. Quantitatively, the latter initial condition does exhibit slightly faster singlet fission, with a time constant of 250 fs.

The results shown here demonstrate that for reasonable initial conditions, the CT character of low-lying states facilitates ultrafast fission dynamics. The presented study also suggests an interesting endeavor towards engineering initial conditions (either structurally or spectroscopically) to maximize singlet fission rates. Another topic of concern related to spectroscopic preparation involves the vibrational degrees of freedom. In particular, if vibrational relaxation in the excited

state manifold out-competes singlet fission, then the new "initial condition" is equilibrated in the S_1 state. Such relaxation can set up a reorganization energy barrier for subsequent fission, thereby inhibiting the process. Such behavior likely cannot be accounted for using weak-coupling Redfield-like perturbation theory, however the modified Redfield theory[45,71] for adiabatic state populations could be readily applied in this regime.

V. CONCLUSIONS

In conclusion, we have extended the treatment of exciton fission presented in Papers I[26] and II[27] to the crystalline case focusing on pentacene as a concrete example. Our theory combines elements of electronic structure theory with a full treatment of the quantum dynamics that result from the coupling of the electronic degrees of freedom to lattice vibrations. A complete discussion of the role of the CT character in the excited states that mediate the fission process has been presented. While some adjustment of parameters constrained by experimental data has been employed (as is standard in excited state electronic structure calculations of large systems[22]), various non-trivial predictions and features emerge from our theoretical approach with no further alterations that lend strong support to the correctness of the framework presented in Papers I,[26] II,[27] and the present paper. These successful predictions include the non-adiabatic to adiabatic crossover predicted in Paper II[27] and discussed above, the magnitude and direction of the Davydov shift, the full polarization-dependence of the absorption spectrum, and the absolute rate of fission in crystalline pentacene. Finally, using the framework presented here, we have also calculated the absorption line shape properties and fission rate in the more challenging case of hexacene, and have confirmed that the calculated properties are in striking agreement with experiment in this case as well.[48]

The ability to treat fission in systems of this size allows us to distinguish the mechanistic features that arise in dimers or in small aggregates from those uniquely associated with bulk systems. Combined with our dimer study in Paper II,[27] we are thus able to make rather general qualitative and quantitative statements about the earliest steps of singlet fission in both finite and periodic systems. While we have used pentacene as a paradigmatic example, the generality of our approach has ramification for the understanding of singlet fission in a wide range of organic materials. Given these successes, we are now in position to use the theoretical apparatus presented in Papers I,[26] II,[27] and this work to explore the possibilities of more exotic fission phenomena such as the potential conversion of the S_1 state into more than two triplet excitons, as well as realistic "inverse design" and optimization of new fissionable materials.

ACKNOWLEDGMENTS

We thank Jeff Neaton, Pierre Darancet, Sahar Sharifzadeh, Joe Subotnik, Garnet Chan, and Eran Rabani for helpful conversations. This work was supported in part by the Center for Re-Defining Photovoltaic Efficiency through Molecule Scale Control, an Energy Frontier Research Center funded by the US Department of Energy, Office of Science, Office of Basic Energy Sciences under Award No. DE-SC0001085. This work was carried out in part at the Center for Functional Nanomaterials, Brookhaven National Laboratory, which is supported by the U.S. Department of Energy, Office of Basic Energy Sciences under Contract No. DE-AC02-98CH10886 (M.S.H). T.C.B. was supported in part by the Department of Energy Office of Science Graduate Fellowship Program (DOE SCGF), made possible in part by the American Recovery and Reinvestment Act of 2009, administered by ORISE-ORAU under Contract No. DE-AC05-06OR23100.

APPENDIX: ON THE USE OF DIABATIC STATES IN SINGLET FISSION

The theoretical framework employed in Paper I,[26] Paper II,[27] and this paper makes use of a physically motivated, real-space tight-binding basis to define electronic configurations and their coupling to vibrational modes of the lattice. The true eigenstates of the electronic Hamiltonian are found via diagonalization. While not defined via a formal diabatization procedure, this basis may be considered an approximate diabatic basis. Such an approach lies at the heart of nearly all successful theories of dynamical processes in condensed phases,[72–74] including the description of charge,[41,75,76] energy,[41,77,78] and spin transport.[79] In addition, the diabatic approach underlies essentially all successful predictions made in the field of singlet fission, as described in Secs. II and V of the present paper. Given these facts, the concerns raised in the recent paper by Feng *et al.*,[30] that the diabatic picture cannot be employed to study singlet fission, are rather surprising and deserve attention.

One of the points raised in Ref. 30 is based on a configuration analysis of the states relevant to singlet fission. The authors find that the initial and final states in the fission process are mixed with states of charge-transfer character, which is in *agreement* with previous work,[2,24,28] as well as that presented here and in Paper II.[27] More specifically, the authors find that the adiabatic S_1 state is composed of configurations largely of FE and CT character (∼80% of total) while the singlet TT state is overwhelmingly composed of configurations of TT and CT character (>90%). However, the authors consider this a failure of the diabatic picture because the lowest-energy diabatic configurations do not sum to 100%. However, this result is not unique to the diabatic approach and simply reflects an (marginally) incomplete basis. Such behavior is to be expected in the development of physically insightful, low-energy Hamiltonians, but it is straightforward to include additional, higher-energy diabatic configurations (in the active-space sense). However, this is not necessary here because the remaining small percentage of configurations would yield a negligible change in the dynamics. Consider the "correct" adiabatic S_1 state, $|S_1\rangle = \alpha|S_1^{(0)}\rangle + (1-\alpha)|X\rangle$, where $|S_1^{(0)}\rangle$ is an approximate adiabatic state, and $|X\rangle$ schematically describes all additional states that are not captured by a FE/CT diabatic framework. In terms of the rate, this missing weight will enter as (at least) the square, such that the importance of the

neglected configurations is roughly $(1-\alpha)^2/\alpha^2 \sim 0.01$ for $\alpha = 0.9$ ($\alpha^2 \approx 0.8$), i.e., two orders of magnitude smaller.

A second argument is presented in Ref. 30 that more directly concerns the diabatic approach and considers the correct dynamics at particular high-symmetry dimer configurations. Specifically, the authors consider a cofacial (D_{2h}) geometry for acene dimers. While this configuration has no relevance for fission in the crystalline acenes,[8,80] it provides an instructive example of the subtleties that arise when considering state transitions in the diabatic and adiabatic bases. To be concrete, consider a simple 2×2 Hamiltonian in a diabatic basis,

$$H = T(P_z, P_R) + \begin{pmatrix} E_1 & V(z,R) \\ V(z,R) & E_2 \end{pmatrix}, \tag{A1}$$

where T is the nuclear kinetic energy operator, E_i are the diabatic energies of the two states (assumed for simplicity to be independent of nuclear configuration), and $V(z, R)$ is the diabatic coupling between the states. We take the z-axis to be perpendicular to the plane of the dimers and the magnitude of z to denote the distance between the molecules, while R schematically denotes coordinates perpendicular to the z-axis. Thus, when $R = 0$, z is the "D_{2h}-scan" coordinate of Ref. 30. If the diabatic basis is chosen to be the "crude adiabatic" basis (defined so as to coincide with the adiabatic basis at the high-symmetry point $R = 0$), then clearly both $V(z, R = 0)$ and $\partial V(z, R = 0)/\partial z$ are identically zero, as pointed out in Ref. 30.

We first calculate the non-adiabatic coupling (NAC) along the z-axis ($R = 0$),

$$A^x_{+,-}(z, R=0) = \left\langle \psi_+ \left| \frac{\partial}{\partial x} \right| \psi_- \right\rangle_{(z,R=0)}, \tag{A2}$$

where x is a nuclear coordinate which can be taken separately as either z or R and $|\psi_\pm\rangle$ are the adiabatic eigenstates of the Hamiltonian, Eq. (A1). Because of the symmetry described above, it is clear that $A^z_{+,-} = 0$, whereas it is straightforward to show that $A^R_{+,-} = \phi(z)/(E_1 - E_2)$, where $\phi(z) \equiv \partial V(z, R)/\partial R|_{R=0}$. While $V(z, R = 0)$ is zero, clearly $\phi(z)$ is not, however $\phi(z)$ will rapidly decay with increasing z.

Physically, the above analysis shows that transitions in the adiabatic picture cannot occur if nuclear motion is constrained to occur along the "D_{2h}-scan" direction, but is facilitated by nuclear motion *transverse* to z along the R directions. Further, because $\phi(z)$ is a decreasing function of z, the probability of transition decreases for increasing molecular separation. We now show that the same physical picture emerges in the diabatic basis. This may seem surprising, because along the z axis ($R = 0$) the mixing between diabatic states $V(z, R)$ is identically zero. However, $V(z, R)$ varies as a function of R as well. In the diabatic picture the facilitator of transitions is the vibronic coupling, found by expansion of $V(z, R)$. To lowest order, $V(z, R) \approx \phi(z)R$, which is closely related to the linear vibronic coupling model frequently employed in the simulation of non-adiabatic processes.[81,82] If we assume for simplicity that z in a non-dynamical parameter (i.e., z is fixed), then the golden-rule transition rate between diabatic states may be written as[83]

$$k = \frac{\phi(z)^2}{\hbar^2} \int_{-\infty}^{\infty} dt e^{i(E_1-E_2)t/\hbar} \langle R(t)R(0)\rangle, \tag{A3}$$

where $\langle R(t)R(0)\rangle$ is the time correlation function of transverse nuclear fluctuations. Despite the difference in precise meaning of electronic transitions in the two bases, the same gross features emerge: (1) a rate for transitions that is zero if nuclear motion is constrained to proceed only along z, (2) a finite rate facilitated by transverse nuclear motion, and (3) a rate that decreases as z increases. With regards to Ref. 30, we emphasize that $V(z, R = 0) = 0$ does not imply $\phi(z) = \partial V(z, R)/\partial R|_{R=0} = 0$. In the adiabatic picture this term provides a non-zero NAC, and in the diabatic picture it defines the strength of the vibronic coupling.

In conclusion, we disagree with the concerns raised by Feng *et al.*[30] regarding the utility of the diabatic basis for singlet fission. Indeed, several studies have very recently appeared, using electronic structure methodologies similar to that employed by Feng *et al.*, that have constructed a diabatic basis starting from numerically determined adiabatic wave functions and have successfully computed fission-related properties.[31,32] Furthermore, a restricted active-space product wavefunction ansatz has very recently been employed by Parker *et al.*[84] to directly construct high-accuracy diabatic states for singlet fission in dimers. These converged calculations have employed the largest active-space to date and have quantitatively confirmed the validity of a diabatic approach to the electronic structure aspect of the problem. The physically-motivated diabatic approach described in Paper I,[26] Paper II,[27] and this work is in semi-quantitative agreement with all of these studies with respect to the description of the electronic structure.

[1] M. B. Smith and J. Michl, Chem. Rev. **110**, 6891 (2010).
[2] M. B. Smith and J. Michl, Annu. Rev. Phys. Chem. **64**, 361 (2013).
[3] J. H. Werner, S. Kolodinksi, and H. J. Queisser, Phys. Rev. Lett. **72**, 3851 (1994).
[4] M. C. Hanna and A. J. Nozik, J. Appl. Phys. **100**, 074510 (2006).
[5] W. Shockley and H. J. Queisser, J. Appl. Phys. **32**, 510 (1961).
[6] J. C. Johnson, A. J. Nozik, and J. Michl, J. Am. Chem. Soc. **132**, 16302 (2010).
[7] J. J. Burdett, A. M. Müller, D. Gosztola, and C. J. Bardeen, J. Chem. Phys. **133**, 144506 (2010).
[8] A. Rao, M. W. B. Wilson, J. M. Hodgkiss, S. Albert-Seifried, H. Bässler, and R. H. Friend, J. Am. Chem. Soc. **132**, 12698 (2010).
[9] J. J. Burdett, D. Gosztola, and C. J. Bardeen, J. Chem. Phys. **135**, 214508 (2011).
[10] W.-L. Chan, M. Ligges, A. Jailaubekov, L. Kaake, L. Miaja-Avila, and X.-Y. Zhu, Science **334**, 1541 (2011).
[11] M. W. B. Wilson, A. Rao, J. Clark, R. S. S. Kumar, D. Brida, G. Cerullo, and R. H. Friend, J. Am. Chem. Soc. **133**, 11830 (2011).
[12] S. T. Roberts, R. E. McAnally, J. N. Mastron, D. H. Webber, M. T. Whited, R. L. Brutchey, M. E. Thompson, and S. E. Bradforth, J. Am. Chem. Soc. **134**, 6388 (2012).
[13] W.-L. Chan, M. Ligges, and X.-Y. Zhu, Nat. Chem. **4**, 840 (2012).
[14] J. J. Burdett and C. J. Bardeen, J. Am. Chem. Soc. **134**, 8597 (2012).
[15] L. Ma, K. Zhang, C. Kloc, H. Sun, M. E. Michel-Beyerle, and G. G. Gurzadyan, Phys. Chem. Chem. Phys. **14**, 8307 (2012).
[16] C. Ramanan, A. L. Smeigh, J. E. Anthony, T. J. Marks, and M. R. Wasielewski, J. Am. Chem. Soc. **134**, 386 (2012).
[17] M. W. B. Wilson, A. Rao, B. Ehrler, and R. H. Friend, Acc. Chem. Res. **46**, 1330 (2013).
[18] M. W. B. Wilson, A. Rao, K. Johnson, S. Gélinas, R. di Pietro, J. Clark, and R. H. Friend, J. Am. Chem. Soc. **135**, 16680 (2013).

[19]J. Lee, M. J. Bruzek, N. J. Thompson, M. Y. Sfeir, J. E. Anthony, and M. A. Baldo, Adv. Mater. **25**, 1445 (2013).
[20]E. C. Greyson, J. Vura-Weis, J. Michl, and M. A. Ratner, J. Phys. Chem. B **114**, 14168 (2010).
[21]P. M. Zimmerman, Z. Zhang, and C. B. Musgrave, Nat. Chem. **2**, 648 (2010).
[22]P. M. Zimmerman, F. Bell, D. Casanova, and M. Head-Gordon, J. Am. Chem. Soc. **133**, 19944 (2011).
[23]P. Teichen and J. D. Eaves, J. Phys. Chem. B **116**, 11473 (2012).
[24]R. W. A. Havenith, H. D. de Grier, and R. Broer, Mol. Phys. **110**, 2445 (2012).
[25]J. C. Johnson, A. J. Nozik, and J. Michl, Acc. Chem. Res. **46**, 1290 (2013).
[26]T. C. Berkelbach, M. S. Hybertsen, and D. R. Reichman, J. Chem. Phys. **138**, 114102 (2013).
[27]T. C. Berkelbach, M. S. Hybertsen, and D. R. Reichman, J. Chem. Phys. **138**, 114103 (2013).
[28]D. Beljonne, H. Yamagata, J. L. Brédas, F. C. Spano, and Y. Olivier, Phys. Rev. Lett. **110**, 226402 (2013).
[29]P. J. Vallet, J. L. Snyder, and N. H. Damrauer, J. Phys. Chem. A **117**, 10824 (2013).
[30]X. Feng, A. V. Luzanov, and A. I. Krylov, J. Phys. Chem. Lett. **4**, 3845 (2013).
[31]D. Casanova, J. Chem. Theory Comput. **10**, 324 (2014).
[32]T. Zeng, R. Hoffmann, and N. Ananth, J. Am. Chem. Soc. **136**, 5755 (2014).
[33]A. M. Müller, Y. S. Avlasevich, K. Müllen, and C. J. Bardeen, Chem. Phys. Lett. **421**, 518 (2006).
[34]A. M. Müller, Y. S. Avlasevich, W. W. Schoeller, K. Müllen, and C. J. Bardeen, J. Am. Chem. Soc. **129**, 14240 (2007).
[35]S. R. Yost, J. Lee, M. W. B. Wilson, T. Wu, D. P. McMahon, R. R. Parkhurst, N. J. Thompson, D. N. Congreve, A. Rao, K. Johnson, M. Y. Sfeir, M. Bawendi, T. M. Swager, R. H. Friend, M. A. Baldo, and T. van Voorhis, Nat. Chem. **6**, 492 (2014).
[36]H. Yamagata, J. Norton, E. Hontz, Y. Olivier, D. Beljonne, J. L. Brédas, R. J. Silbey, and F. C. Spano, J. Chem. Phys. **134**, 204703 (2011).
[37]W.-L. Chan, T. C. Berkelbach, M. R. Provorse, N. R. Monahan, J. R. Tritsch, M. S. Hybertsen, D. R. Reichman, J. Gao, and X.-Y. Zhu, Acc. Chem. Res. **46**, 1321 (2013).
[38]S. Sharifzadeh, P. Darancet, L. Kronik, and J. B. Neaton, J. Phys. Chem. Lett. **4**, 2197 (2013).
[39]P. Petelenz and B. Pac, J. Am. Chem. Soc. **135**, 17379 (2013).
[40]H.-P. Breuer and F. Petruccione, *The Theory of Open Quantum Systems* (Oxford University Press, 2002).
[41]V. May and O. Kühn, *Charge and Energy Transfer Dynamics in Molecular Systems* (Wiley-VCH, 2011).
[42]A. G. Redfield, Adv. Magn. Reson. **1**, 1 (1965).
[43]V. Novoderezhkin, J. M. Salverda, H. van Amerongen, and R. van Grondelle, J. Phys. Chem. B **107**, 1893 (2003).
[44]V. I. Novoderezhkin, M. A. Palacios, H. van Amerongen, and R. van Grondelle, J. Phys. Chem. B **108**, 10363 (2004).
[45]M. Yang and G. R. Fleming, Chem. Phys. **282**, 163 (2002).
[46]S. Jang, Y.-C. Cheng, D. R. Reichman, and J. D. Eaves, J. Chem. Phys. **129**, 101104 (2008).
[47]S. Jang, T. C. Berkelbach, and D. R. Reichman, New J. Phys. **15**, 105020 (2013).
[48]E. Busby, T. C. Berkelbach, B. Kumar, A. Chernikov, Y. Zhong, X.-Y. Zhu, T. F. Heinz, M. S. Hybertsen, M. Y. Sfeir, D. R. Reichman, C. Nuckolls, and O. Yaffe, J. Am. Chem. Soc. **136**, 10486 (2014).
[49]W. T. Pollard and R. A. Friesner, J. Chem. Phys. **100**, 5054 (1994).
[50]M. L. Tiago, J. E. Northrup, and S. G. Louie, Phys. Rev. B **67**, 115212 (2003).
[51]E. A. Silinsh, V. A. Kolesnikov, I. J. Muzikante, and D. R. Balode, Phys. Status Solidi B **113**, 379 (1982).
[52]F. Amy, C. Chan, and A. Kahn, Org. Electron. **6**, 85 (2005).
[53]*NIST Chemistry WebBook*, NIST Standard Reference Database Number 69, edited by P. L. Linstrom and W. G. Mallard (National Institute of Standards and Technology, Gaithersburg MD, 2014).
[54]M. Rohlfing and S. G. Louie, Phys. Rev. B **62**, 4927 (2000).
[55]D. Biermann and W. Schmidt, J. Am. Chem. Soc. **102**, 3163 (1980).
[56]S. Murov, I. Carmichael, and G. Hug, *Handbook of Photochemistry* (Marcel Dekker, New York, 1993).
[57]L. Sebastian, G. Weiser, and H. Bässler, Chem. Phys. **61**, 125 (1981).
[58]M. Grobosch, R. Schuster, T. Pichler, M. Knupfer, and H. Berger, Phys. Rev. B **74**, 155202 (2006).
[59]M. Dressel, B. Gompf, D. Faltermeier, A. K. Tripathi, J. Pflaum, and M. Schubert, Opt. Express **64**, 19770 (2008).
[60]F. Roth, R. Schuster, A. König, M. Knupfer, and H. Berger, J. Chem. Phys. **136**, 204708 (2012).
[61]F. Roth, B. Mahns, S. Hampel, M. Nohr, H. Berger, B. Büchner, and M. Knupfer, Eur. Phys. J. B **86**, 66 (2013).
[62]A. F. Prikhoto and L. I. Tsikora, Opt. Spectrosc. **25**, 242 (1968).
[63]D. Faltermeier, B. Gompf, M. Dressel, A. K. Tripathi, and J. Pflaum, Phys. Rev. B **74**, 125416 (2006).
[64]V. Zanker and J. Preuss, Z. Angew. Phys. **27**, 363 (1969).
[65]P. Cudazzo, M. Gatti, and A. Rubio, Phys. Rev. B **86**, 195307 (2012).
[66]Y. K. Shin, B. S. Brunschwig, C. Creutz, and N. Sutin, J. Am. Chem. Soc. **117**, 8668 (1995).
[67]M. W. Schmidt, K. K. Baldridge, J. A. Boatz, S. T. Elbert, M. S. Gordon, J. H. Jensen, S. Koseki, N. Matsunaga, K. A. Nguyen, S. Su, T. L. Windus, M. Dupuis, and J. A. Montgomery, J. Comput. Chem. **14**, 1347 (1993).
[68]R. L. Martin, J. Chem. Phys. **118**, 4775 (2003).
[69]A. Troisi and G. Orlandi, J. Phys. Chem. B **109**, 1849 (2005).
[70]C. Ambrosch-Draxl, D. Nabok, P. Puschnig, and C. Meisenbichler, New J. Phys. **11**, 125010 (2009).
[71]W. M. Zhang, T. Meier, V. Chernyak, and S. Mukamel, J. Chem. Phys. **108**, 7763 (1998).
[72]M. Baer, Chem. Phys. Lett. **35**, 112 (1975).
[73]M. D. Newton, Chem. Rev. **91**, 767 (1991).
[74]T. van Voorhis, T. Kowalczyk, B. Kaduk, L.-P. Wang, C.-L. Cheng, and Q. Wu, Annu. Rev. Phys. Chem. **61**, 149 (2010).
[75]T. Holstein, Ann. Phys. **8**, 325 (1959).
[76]R. A. Marcus, Annu. Rev. Phys. Chem. **15**, 155 (1967).
[77]T. Förster, Discuss. Faraday Soc. **27**, 7 (1959).
[78]D. L. Dexter, J. Chem. Phys. **21**, 836 (1953).
[79]G. D. Mahan, *Many-Particle Physics* (Kluwer Academic/Plenum Publishing, 2000).
[80]T. S. Kuhlman, J. Kongsted, K. V. Mikkelsen, K. B. Møller, and T. I. Sølling, J. Am. Chem. Soc. **132**, 3431 (2010).
[81]H. Köppel, W. Domcke, and L. S. Cederbaum, Adv. Chem. Phys. **57**, 59 (1984).
[82]G. A. Worth and L. S. Cederbaum, Annu. Rev. Phys. Chem. **55**, 127 (2004).
[83]R. Zwanzig, *Nonequilibrium Statistical Mechanics* (Oxford University Press, 2001).
[84]S. M. Parker, T. Seideman, M. A. Ratner, and T. Shiozaki, J. Phys. Chem. C **118**, 12700 (2014).